Front. Phys. 12(3), 128701 (2017)
DOI 10.1007/s11467-017-0665-y

RESEARCH ARTICLE

Ordered quasi-two-dimensional structure of nanoparticles in semiflexible ring polymer brushes under compression

Yunfeng Hua, Zhenyu Deng, Yangwei Jiang, Linxi Zhang†

Department of Physics, Zhejiang University, Hangzhou 310027, China
Corresponding author. E-mail: †*lxzhang@zju.edu.cn*
Received October 25, 2016; accepted December 29, 2016

Molecular dynamics simulations of a coarse-grained bead-spring model of ring polymer brushes under compression are presented. Flexible polymer brushes are always disordered during compression, whereas semiflexible polymer brushes tend to be ordered under sufficiently strong compression. Further, the polymer monomer density of the semiflexible polymer brush is very high near the brush surface, inducing a peak value of the free energy near the surface. Therefore, when nanoparticles are compressed in semiflexible ring polymer brushes, they tend to exhibit a closely packed single-layer structure between the brush surface and the impenetrable wall, and a quasi-two-dimensional ordered structure near the brush surface is formed under strong compression. These findings provide a new approach to designing responsive applications.

Keywords molecular dynamics simulation, semiflexible ring polymer brushes, nanoparticle, compression, ordered structure

PACS numbers 87.10.Tf, 87.10.Pq, 87.15.hp

Frontiers of Physics

1 Introduction

Two-dimensional (2D) nanomaterials are an interesting class of materials whose surface area is dominated by one specific crystallographic plane; therefore, they are almost crystallographically isotropic. Referred to in the literature by various names such as nanoflakes [1], nanowalls [2], nanosheets [3, 4], nanoplates, or nanoplatelets [5–7], 2D inorganic nanomaterials (not to be confused with 2D carbon-based nanomaterials such as graphene [8]), are typically nanoscale in one dimension yet microscale in the other two. The use of 2D layered materials has been attracting particular interest recently because of their unique electronic, structural, and optical properties [9, 10] and has quickly become one of the hottest research topics [11–13]. Compared with zero-dimensional and one-dimensional materials, 2D layered materials have several extraordinary advantages [14] that endow them with promising potential for solar energy harvesting and photocatalytic applications [15–19]. For instance, 2D layered materials with high specific surface areas could provide a great number of active sites for various reactions. Additionally, nanosized 2D layered materials could act as a support for fabrication of various composites with a large interfacial contact [10, 20].

Further, grafted polymeric layers, usually called polymer brushes, are currently used as surface modifiers and have been the subject of intensive investigation for several decades. Owing to the delicate interplay between the configurational entropy of these polymers, the excluded volume, and the (solvent-mediated) enthalpic interactions, the structure of these soft polymeric layers and their response to external perturbations is characterized by very diverse, complex, and rich properties [21–23]. Although polymer brushes are used for various applications [24], certain aspects of the complex behavior of such systems are not yet well understood, and more research is still needed to clarify them.

In this paper, we simulate the 2D structure of nanoparticles (NPs) induced by compressing the NPs in a ring polymer brush system. Polymers are adopted to control the effective interactions between NPs and further

*Special Topic: Soft-Matter Physics and Complex Systems (Ed. Zhi-Gang Zheng). arXiv: 1701.05659.

govern the assembly structures of the NPs. Section 2 presents the model and simulation method, and Section 3 describes the resulting density profiles, system pressure, polymer structure, order parameter under various degrees of compression, and ordered structures of the NPs. In Section 4, we briefly present our conclusions.

2 Model and simulation methods

We employ molecular dynamics simulations based on a coarse-grained model to study the conformations of pure ring polymer brushes and the ordered structure of NPs in ring polymer brushes under compression. Polymer chains are grafted uniformly on an impenetrable surface with a grafting density σ_g, and each chain consists of $N_m = 120$ monomers. In fact, similar results can also be obtained for ring polymer brushes with random grafting on the surface. The number of NPs is fixed at $N_p = 90$. To prevent overlap between any two monomers in the system, a purely repulsive truncated and shifted Lennard–Jones potential is used:

$$U_{LJ}(r_{ij}) = \begin{cases} 4\varepsilon\left[\left(\frac{\sigma}{r_{ij}}\right)^{12} - \left(\frac{\sigma}{r_{ij}}\right)^{6}\right] + \frac{1}{4}, & 0 < r_{ij} < 2^{1/6}\sigma, \\ 0, & r_{ij} \geq 2^{1/6}\sigma, \end{cases} \quad (1)$$

where r_{ij} is the spatial distance between monomers, σ is the monomer diameter, and $\varepsilon = k_B T$ (where k_B is the Boltzmann constant, and T is the temperature of the system). Here, the monomer diameter of the polymer brushes is $\sigma_m = \sigma$, and the diameter of the NPs is fixed at $\sigma_p = 3\sigma$. We set the mass of the brush monomer to m, and the mass of the NPs is $(\sigma_p/\sigma)^3$ times the brush monomer mass.

All the bonded monomers in the polymer brushes interact with the well-known finitely extensible nonlinear elastic potential [25]

$$V_{FENE} = -\frac{KR_0^2}{2} \ln\left[1 - \left(\frac{r}{R_0}\right)^2\right], \quad r < R_0, \quad (2)$$

where r is the distance between two bonded monomers, $K = 30\varepsilon/\sigma^2$ is the spring constant, and $R_0 = 1.5\sigma$ is the maximum distance between bonded monomers [25].

The stiffness of the polymer chain is described by the angle bending potential [26–28]:

$$U_b = k_b(1 + \cos\theta), \quad (3)$$

where θ is the angle between two consecutive bonds, and k_b denotes the bending stiffness.

The polymer brushes are grafted on a planar $30\sigma \times 26\sigma$ impenetrable surface with a dense uniform lattice arrangement of grafting sites. The substrate surface exerts a purely repulsive truncated and shifted Lennard-Jones potential described by Eq. (4) for all the monomers, and the parameters are chosen as $\sigma_{surface} = \sigma$ (the diameter of the surface monomer) and $\varepsilon = k_B T$ as in Eq. (4). Further, the surface is infinitely extended through periodic boundary conditions in the xy plane. At the beginning of the simulation, the distance between two impenetrable surfaces is $d = 80\sigma$, and NPs are located randomly outside the brush. The grafting surface is immobile, and the compression surface is slowly pressed toward the grafting surface during the compression process. The molecular dynamics simulations are realized by using the Langevin dynamics approach with the open-source software LAMMPS [29] under a reduced temperature, $T^* = k_B T/\varepsilon = 1.0$. Reduced units of $\varepsilon = 1.0$, $\sigma = 1.0$, and $m = 1.0$ are used to represent the energy, length, and mass, respectively. The time unit τ and friction coefficient γ in the molecular dynamics simulations of a Langevin thermostat are set to $0.001\tau_0$ and $1/\tau_0$, respectively, where $\tau_0 = \sqrt{m\sigma^2/\varepsilon}$ is the time unit in our simulation. A series of simulations with various chain stiffnesses (k_b) and grafting densities (σ_g) are performed. Data are obtained from an equilibrium time of about $1 \times 10^7\tau$ for each case, and the total simulation time for each run is about $3.5 \times 10^7\tau$. The statistical data presented below are averaged over a sufficient number of samples, and the errors of the ensemble averages are not shown in the figures because they are smaller than the symbols. All the simulation snapshots are captured via the Visual Molecular Dynamics package [30].

3 Results and discussion

3.1 Compression-driven conformations of semiflexible ring brushes

The compression processes of ring polymer brushes are investigated. Two typical snapshots of ring polymer brushes with a grafting density of $\sigma_g = 0.11$ are shown in Fig. 1. As indicated, flexible ring polymer brushes with $k_b = 0$ (a and c) and semiflexible ring polymer brushes with $k_b = 160$ (b and d, from two different side views) under compression characterized by the degree of compression, $D/h_0 = 1.0$ (a and b) and $D/h_0 = 0.5$ (c and d), are displayed. Here, D is the distance between the two planes, and h_0 is the average height of the polymer brushes without compression, which is defined from when $\phi(z)$ (see Fig. 2) has decreased to about 50% of its original value in the flat region of $\phi(z)$. We set $h_0 \approx 40\sigma$ for the flexible ring polymer brush and $h_0 \approx 45\sigma$ for the flexible ring polymer. In Figs. 1(a) and (c), flexible chains always have a disorderly distribution, and the density increases gradually as the degree of compression increases. In contrast, the semiflexible ring chains have

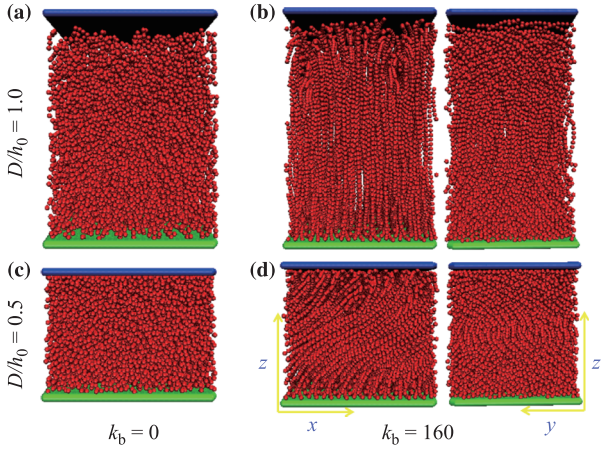

Fig. 1 Snapshots of ring polymer brushes for $\sigma_g = 0.11$ with $k_b = 0$ **(a, c)** and $k_b = 160$ (**b** and **d**, from two different side views) under compression characterized by $D/h_0 = 1.0$ (a, b) and $D/h_0 = 0.5$ (c, d). Here k_b denotes the bending stiffness, σ_g is the grafting density of the polymer brushes, D is the distance between the two planes, and h_0 is the average height of the polymer brushes without compression.

much more orderly distributions. In the xz plane, the distribution of the ring polymer brush is similar to that of the semiflexible linear polymer brush shown in our previous work [31]. In the yz plane, ring-like structures induced by chain stiffness are observed, indicating that the monomer density along the z direction near the two impenetrable surfaces is greater than that in the central region.

The density profiles $\phi(z)$ of the total monomer density for flexible ring brushes [Fig. 2(a)] and semiflexible ring brushes [Fig. 2(b)] under various degrees of compression are shown in Fig. 2. Here, z is the distance between the brush monomer and the grafting surface along the z direction, and $\phi(z)$ is the monomer density in the range from z to $z + \Delta z$ (where Δz is set to 0.5σ). In Fig. 2(a), the monomer density profiles for ring polymer brushes and linear polymer brushes [31] are almost identical. For flexible ring polymer brushes with $k_b = 0$, compression can lead to pronounced layering of the monomers near the grafting surface. At the brush surface, the parabolic decay of the density profiles found in the free ring polymer brushes is replaced by density oscillations in the compressed ring polymer brushes, whereas for a large k_b of 160, remarkable differences are found. There is no layering of the monomers, and the density distribution $\phi(z)$ near the two walls is extremely high, resulting in a high free energy near the chain surfaces. The corresponding arrangement of semiflexible ring polymer brushes under compression is shown in the inset.

To illustrate the conformations of the ring polymer brushes during compression, Fig. 3 shows the variation of the angle $\theta_{i,i+1}$ of consecutive bonds along the ring chain backbone at various degrees of compression D/h_0. Figure 4 shows the density distributions of the angle $\varphi_{i-1,i,i+1}$ between neighboring bonds $\rho(\varphi)$ and the angle $\theta_{i,i+1}$ of consecutive bonds $\rho(\theta)$ at different degrees of compression D/h_0 for both the linear polymer brush and ring polymer brush. Here, the monomers are labeled consecutively $i = 1, 2, \ldots$, starting at the grafting monomer,

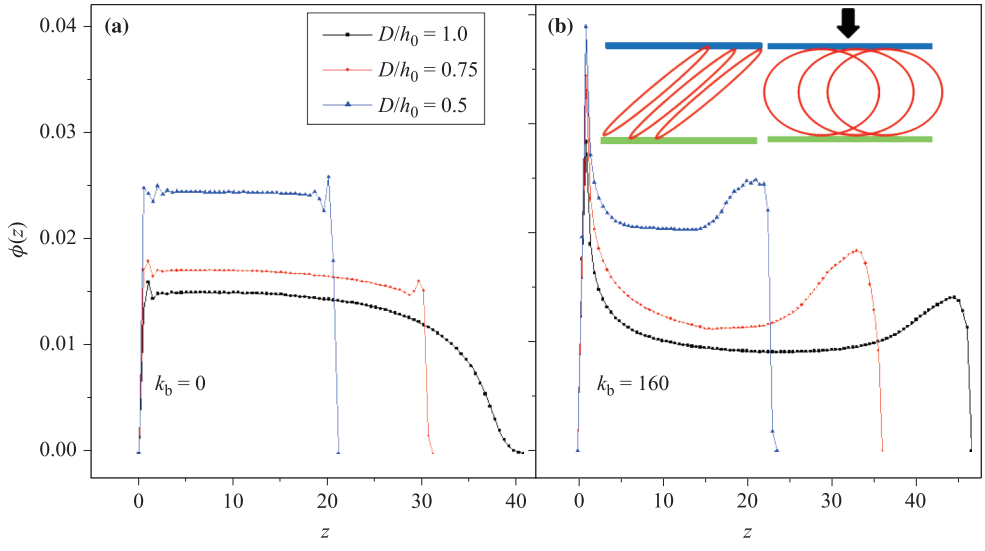

Fig. 2 Density distribution of the effective monomers in the brush, $\Phi(z)$, vs. distance z from the grafting surface for $D/h_0 = 1.0$, 0.75, and 0.5. Two values of k_b are considered: **(a)** a flexible ring polymer ($k_b = 0$) and **(b)** a semiflexible ring polymer ($k_b = 160$). Inset shows the corresponding arrangement of semiflexible brushes in the xy plane. The number of monomers per ring chain is N_m, and $\sigma_g = 0.11$.

and $\theta_{i,i+1}$ is the angle between the i-th bond vector and the z_0 vector (the unit vector along the z direction). The angle $\theta_{i,i+1}$ in Fig. 3 is obtained from 5000 samples, each of which consists of 100 polymer chains (here, the index i runs from 1 to 120; if $i = 120$, $\theta_{i,i+1}$ represents $\theta_{i,1}$). For flexible ring brushes with $k_b = 0$, the angle $\theta_{i,i+1}$ increases slowly from $i = 0$–50 and $i = 70$–120. However, from $i = 50$–70, $\theta_{i,i+1}$ increases dramatically. Furthermore, a higher degree of compression results in a more dramatic increase in $\theta_{i,i+1}$. For $k_b = 160$, a likely trigonometric trend is found. For $D/h_0 = 1.0$, $\theta_{i,i+1}$ varies gradually from $\pi/2$ to 0, then to π, and finally from π to $\pi/2$, indicating a circular structure. For comparison, the result for semiflexible linear chains with $k_b = 160$ are displayed in the inset; it is completely different from that for semiflexible ring chains. The polar angle $\theta_{i,i+1}$ for semiflexible linear chains is almost independent of the monomer index i when $D/h_0 = 1.0$, whereas for $D/h_0 = 0.5$, $\theta_{i,i+1}$ first gradually increases and then remains constant.

In Fig. 4, the angle profile between neighboring bonds $\rho(\varphi)$ varies little during compression for both semiflexible linear brushes and semiflexible ring brushes. For ring polymer brushes, the distribution of the bending energy along the chain backbone is approximately uniform. $\varphi_{i-1,i,i+1}$ is almost constant, and $\rho(\varphi)$ is concentrated in a very small range. For flexible ring polymer brushes, compression causes the density profile of $\varphi_{i-1,i,i+1}$ to shift rightward, and $\varphi_{i-1,i,i+1}$ increases as the degree of compression increases. The density profile of $\rho(\varphi)$ for the semiflexible linear polymer brush is shifted slightly rightward under stronger compression. For the flexible ring brush with $k_b = 0$, the density profile $\rho(\theta)$ oscillates, and the density profile varies from two peaks to just one

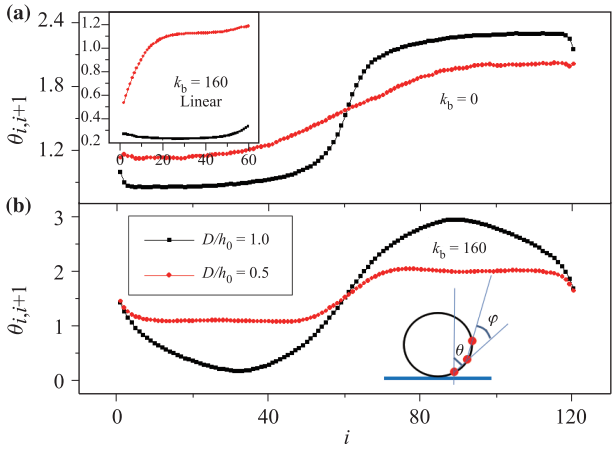

Fig. 3 Variation of the angle $\theta_{i,i+1}$ between two consecutive bonds along the ring chain backbone as well as the normal to the grafting surface under different degrees of compression D/h_0 for **(a)** flexible ring polymer ($k_b = 0$) and **(b)** semiflexible ring polymer ($k_b = 160$). Inset shows the result for semiflexible linear chains for $k_b = 160$.

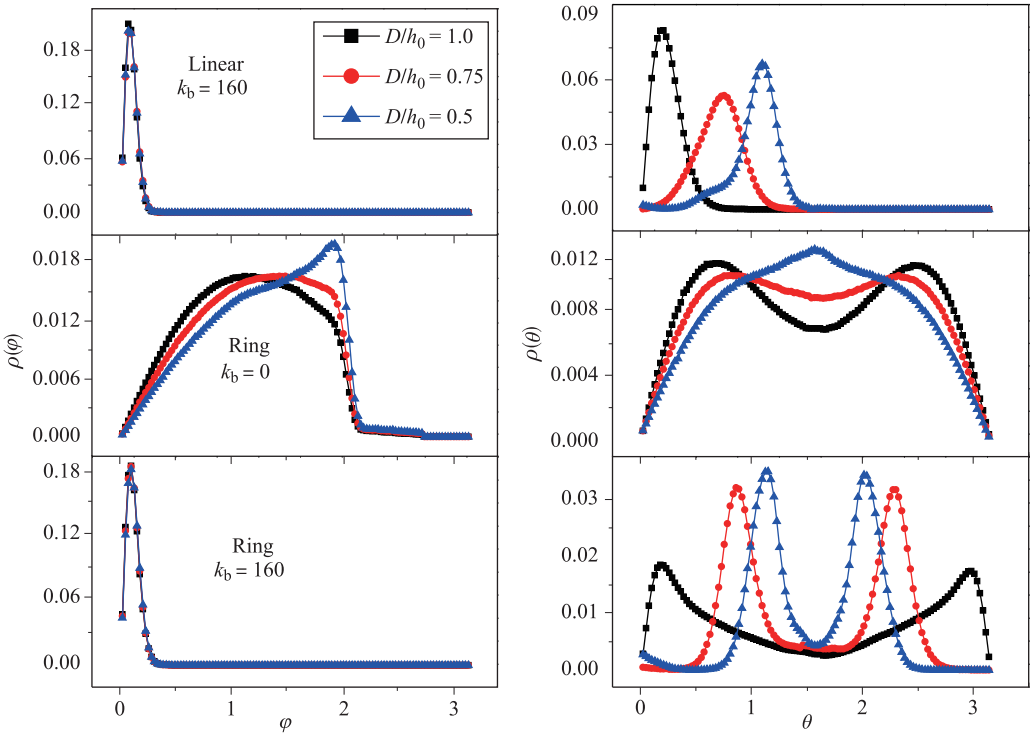

Fig. 4 Density distribution of the angle $\varphi_{i-1,i,i+1}$between neighboring bonds $\rho(\varphi)$ and the angle $\theta_{i,i+1}$ of consecutive bonds $\rho(\theta)$ at different degrees of compression D/h_0 for linear and ring chains.

as D/h_0 reaches 0.5. For the semiflexible ring brush with $k_b = 160$, the two peak values of the density profile $\rho(\theta)$ become larger under stronger compression, and the θ values for $D/h_0 = 0.5$ corresponding to the peak values ($\theta \approx 1.1$ and 2.0) are perfectly matched with those in Fig. 3.

A particularly useful quantity for describing the conformations of polymer chains is the order parameter,

$$S = \frac{1}{2}(3\langle\cos^2\theta'\rangle - 1), \tag{4}$$

where θ' denotes the angle between the middle bond vector $\theta'_{j_{xy}}$ (the projection of the bond between $i = N_m/2 = 60$ and $i' = i + 1 = 61$ in the xy plane) of the chain and θ'_0, here

$$\theta'_0 = \frac{1}{N_{\text{chain}}}\sum_{j=1}^{N_{\text{chain}}}\theta'_{j_{xy}}. \tag{5}$$

The order parameters for flexible and semiflexible ring brushes under various degrees of compression are shown in Fig. 5. The order parameter for the flexible brush obviously remains about 0.25, whereas for the semiflexible brush, the order parameter increases as the degree of compression increases ($S \approx 0.9$ when $D/h_0 = 0.5$). The flexible brush is always disordered regardless of how much the system is compressed; however, for the semiflexible brush, the order parameter increases rapidly at $D/h_0 = 1.0$ ($S \approx 0.35$–0.8) and finally maintains a stable value. One can conclude that compression strongly affects the semiflexible brush system, rendering it more ordered.

In Fig. 6, we show the pressure exerted by a brush of ring polymers with various stiffnesses as well as linear polymers at height D above the grafting plane. For flexible brushes, the pressure increases gradually during compression, which is in good agreement with the results of Milchev and Binder [32]. However, the trend for semiflexible brushes is completely different; a dramatic increase to a maximum followed by a steady plateau is observed. Under strong compression, the pressure of the semiflexible brushes is smaller than that of the flexible brushes. Furthermore, the peak value of the pressure profile is smaller for semiflexible ring brushes than for semiflexible linear brushes, whereas the pressure for ring brushes is greater than that for linear brushes under strong compression. The inset shows schematic illustrations of the compression process. Semiflexible linear brushes are quickly tilted under stronger compression. Deformation of semiflexible ring brushes occurs at a small degree of compression ($D/h_0 > 0.92$), and tilting follows as the degree of compression increases.

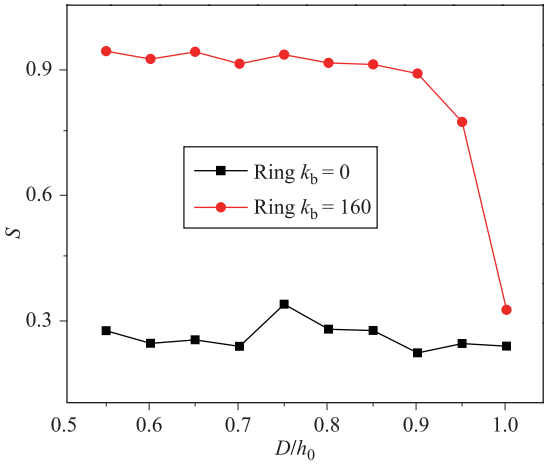

Fig. 5 Order parameter S of the orientation of the bond between the 59$^{\text{th}}$ and 60$^{\text{th}}$ monomers in polymer brushes (represented by unit vectors in the xy plane) vs. D/h_0 for flexible and semiflexible ring brushes. Here $N_m = 120$, and $\sigma_g = 0.11$.

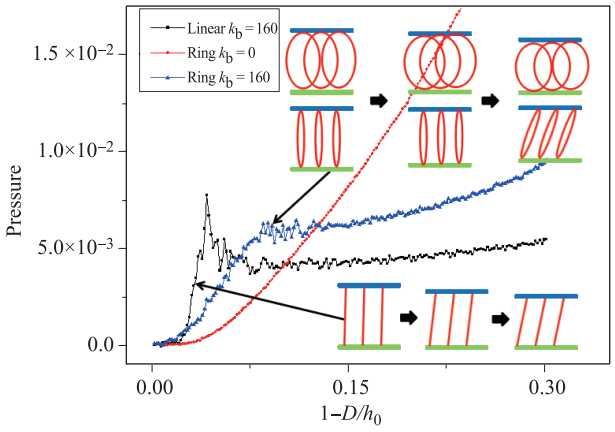

Fig. 6 Pressure P along z direction vs. the degree of compression, $1 - D/h_0$, for ring brush with chain length $N_m = 120$, grafting density $\sigma_g = 0.11$ (both flexible and semiflexible brushes are included) and linear brush with $N_m = 60$, $\sigma_g = 0.22$. Schematic shows the transformation of polymer brushes during compression.

3.2 Ordered structures for nanoparticles in semiflexible ring polymer brushes

Owing to the nontrivial monomer density distribution of semiflexible ring polymer brushes, one may obtain ordered structures of NPs by compressing NPs on the brush surface. Figure 7 shows the conformations of NPs in ring polymer brushes at various degrees of compression, $D/h_0 = 1.0$ (a and b) and $D/h_0 = 0.5$ (c and d). For both flexible and semiflexible ring brushes, all the NPs accumulate near the polymer brush surface during compression. For flexible ring polymer brushes, NPs are randomly located at the brush surface owing to the uniform distribution of the polymer ring brush and the

gradual increase in the polymer brush density. In contrast, for semiflexible ring polymer brushes, because the monomer density is higher near the polymer surface, NPs are closely packed in a single layer. In addition, for a larger degree of compression, the NPs exhibit more orderly packing. The quasi-2D ordered structure of the NPs is highly important in various applications, as it improves the scratch resistance, exposes catalytic components for bioreactions, and inhibits dewetting from the low-energy substrate.

To analyze the distribution of NPs in more detail, we plot the density profiles of NPs, $\rho_n(z)$, as a function of z for the linear brush and ring polymer brush at $D/h_0 = 1.0$, 0.75, and 0.5. The results are shown in Fig. 8. We set $h_0 \approx 58\sigma$ for the semiflexible linear brush with $N_\mathrm{m} = 60$ and $\sigma_g = 0.22$. The compression surface is shown in Fig. 8, where the arrowhead indicates that the system is compressed from right to left. The result for semiflexible linear polymer brushes is in good agreement with our previous work [31]. When the surface is compressed to $D/h_0 = 1.0$, NPs penetrate the brush and are uniformly distributed in the brush, whereas at a large degree of compression, $D/h_0 = 0.5$, NPs are aggregated near the two impenetrable surfaces. For ring brushes, the density profile is in good agreement with the snapshots shown in Fig. 7. All the NPs are located between the polymer brush surface and the compression surface. As

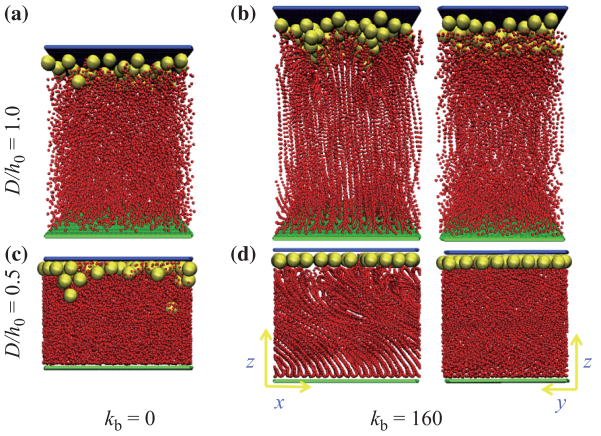

Fig. 7 Snapshots showing the conformations of NPs in ring polymer brushes for $N_\mathrm{m} = 120$, $\sigma_\mathrm{g} = 0.11$, and $k_\mathrm{b} = 0$ **(a, c)** and $k_\mathrm{b} = 160$ (**b** and **d**, from two different side views).

the degree of compression increases, the NPs are packed in a single layer in semiflexible ring brushes. However, in flexible ring polymer brushes, the NPs are randomly located near the brush surface, regardless of the degree of compression.

Figure 9 shows the radial distribution functions between NPs in the single layer near the compression surface. NPs are packed more closely and in a more or-

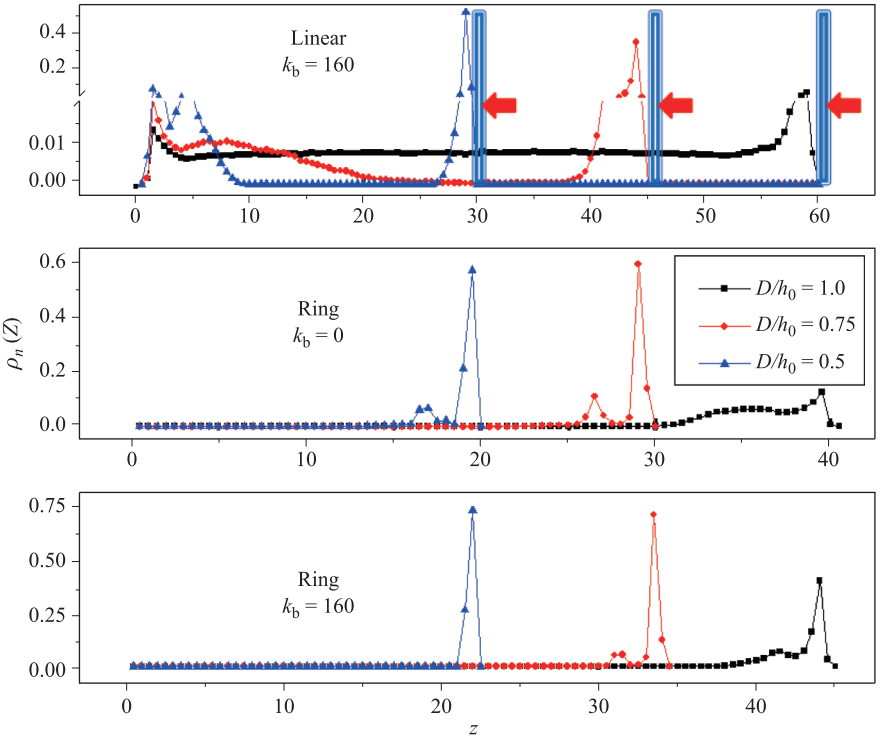

Fig. 8 Density distributions of NPs $\rho_n(z)$ as a function of z for linear brush and ring polymer brushes at $D/h_0 = 1.0, 0.75,$ and 0.5.

derly fashion for $k_b = 160$, and the largest peak value for $g(r_{xy})$ is much greater than that for $k_b = 0$. Further, as shown in the inset, because the diameter of the NPs is $\sigma_p = 3\sigma$, if the NPs are closely arranged, the peak values should occur at $r_{xy} = 3.0, 5.2, 6.0$, and 7.9. The values corresponding to the peak of the $g(r_{xy})$ profile appear at $r_{xy} = 3.05, 5.35, 6.15$, and 8.15, further indicating a highly ordered structure of NPs for $k_b = 160$.

Finally, the free energy of a single NP in the semiflexible ring polymer brushes is calculated via the umbrella sampling method [33], as shown in Fig. 10, where the unit of free energy is k_BT. The minimum free energy of the system is located near the compression surface, which explains why NPs prefer to stay near the compression surface. The result for linear polymer brushes is also shown for comparison. For the linear polymer brush system, there is a free-energy barrier in the central region between the two impenetrable surfaces and a free-energy well near the grafting surface in the free-energy landscape of an NP within linear polymer brushes. The height of the free-energy barrier and the depth of the free-energy well depend mainly on the degree of compression of the two impenetrable surfaces; therefore, NPs can penetrate the linear polymer brushes when compression begins, and they ultimately stay near the two impenetrable walls. However, for the ring polymer brush system, the NPs cannot penetrate the polymer brushes because of the high free-energy barrier at the interface surface. The calculated error estimates for free energy are also shown in Fig. 10. Therefore, the aggregation behaviors of the NPs near the ring polymer brush interface can be well understood in terms of the free-energy landscape.

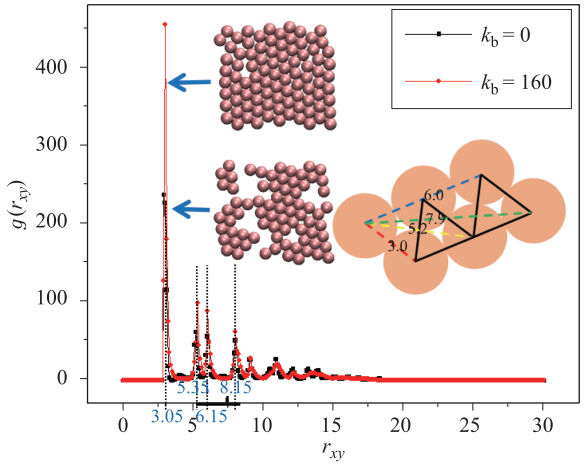

Fig. 9 Pair distribution functions $g(r_{xy})$ between NPs in the first layer close to the compression surface vs. the distance between NPs r_{xy}. Inset shows the arrangement of NPs in the first layer, and the schematic shows the distances corresponding to the peak values of $g(r_{xy})$.

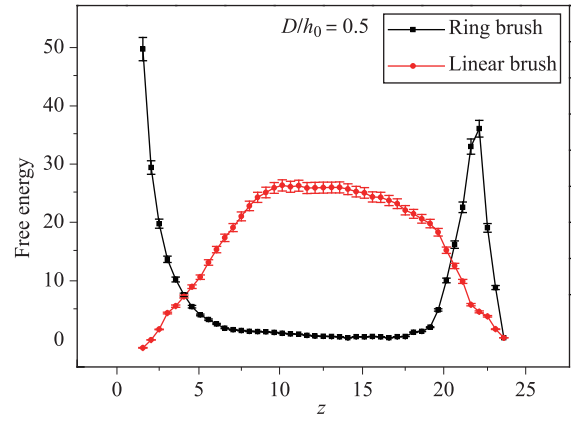

Fig. 10 Free energy $F(z)$ for one NP in semiflexible ring polymer brushes with $k_b = 160$ at $D/h_0 = 0.5$. The result for linear polymer brushes is shown for comparison.

4 Conclusion

Extensive simulations of flexible and semiflexible ring polymer brushes under compression were presented. Flexible ring polymer brushes are disordered, whereas semiflexible ring polymer brushes tend to tilt and exhibit an ordered structure under a sufficient degree of compression. Further, the monomer density near the ring polymer brush is extremely high, which yields a peak value of the free energy. Therefore, NPs cannot penetrate the ring polymer brush and form a quasi-2D ordered structure near the brush surface under strong compression; this finding provides a new approach to designing quasi-2D materials.

Acknowledgements This research was financially supported by the National Natural Science Foundation of China (Grant Nos. 21374102, 21674082, and 21674096). We are grateful to the reviewers of our manuscript for their detailed and insightful comments and suggestions.

References

1. M. V. Reddy, T. Yu, C. H. Sow, Z. X. Shen, C. T. Lim, G. V. S. Rao, and B. V. R. Chowdari, α-Fe_2O_3 nanoflakes as an anode material for Li-ion batteries, *Adv. Funct. Mater.* 17(7), 2792 (2006)

2. T. Yu, Y. W. Zhu, X. J. Xu, Z. X. Shen, P. Chen, C.T. Lim, J. T. L. Thong, and C. H. Sow, Controlled growth and field-emission properties of cobalt oxide nanowalls, *Adv. Mater.* 17(13), 1595 (2005)

3. X. D. Gao, X. M. Li, W. D. Yu, F. Peng, and C. Y. Zhang, Oversized hexagonal nanosheets of layered zinc

hydroxysulfates via the hexamethylenetetraminemediated solution route, *Mater. Res. Bull.* 41(3), 608 (2006)

4. X. Huang, S. Tang, X. Mu, Y. Dai, G. Chen, Z. Zhou, F. Ruan, Z. Yang, and N. Zheng, Freestanding palladium nanosheets with plasmonic and catalytic properties, *Nat. Nanotechnol.* 6(1), 28 (2011)
5. H. L. Wang, H. S. Casalongue, Y. Y. Liang, and H. J. Dai, $NiOH_2$ nanoplates grown on graphene as advanced electrochemical pseudocapacitormaterials, *J. Am. Chem. Soc.* 132(21), 7472 (2010)
6. S. H. Chen and D. L. Carroll, Silver nanoplates: Size control in two dimensions and formation mechanisms, *J. Phys. Chem. B* 108(18), 5500 (2004)
7. X. P. Sun, S. J. Dong, and E. Wang, Large-scale synthesis of micrometer- scale single-crystalline Au plates of nanometer thickness by a wet-chemical route, *Angew. Chem. Int. Ed.* 43(46), 6360 (2004)
8. A. K. Geim, Graphene: Status and prospects, *Science* 324(5934), 1530 (2009)
9. M. Q. Yang, N. Zhang, M. Pagliaro, and Y. J. Xu, Artificial photosynthesis over graphene-semiconductor composites: Are we getting better? *Chem. Soc. Rev.* 43(24), 8240 (2014)
10. S. Z. Butler, S. M. Hollen, L. Cao, Y. Cui, J. A. Gupta, et al., Challenges and opportunities in two-dimensional materials beyond graphene, *ACS Nano* 7(4), 2898 (2013)
11. J. Yu, Y. Yu, P. Zhou, W. Xiao, and B. Cheng, Morphology dependent photocatalytic H_2-production Activity of CdS, *Appl. Catal. B* 184(2), 156 (2014)
12. F. Dong, L. Wu, Y. Sun, M. Fu, Z. Wu, and S. C. Lee, Efficient synthesis of polymeric g-C_3N_4 layered materials as novel efficient visible light driven photocatalysts, *J. Mater. Chem.* 21(39), 15171 (2011)
13. J. Hong, Y. Wang, Y. Wang, W. Zhang, and R. Xu, Noble-metal-free NiS/C_3N_4 for efficient photocatalytic hydrogen evolution from water, *ChemSusChem* 6(12), 2263 (2013)
14. X. Song, J. Hu, and H. Zeng, Two-dimensional semiconductors: Recent progress and future perspectives, *J. Mater. Chem.* 1, 2952 (2013)
15. S. Khanchandani, S. Kundu, A. Patra, and A. K. Ganguli, Shell thickness dependent photocatalytic properties of ZnO/CdS core-shell nanorods, *J. Phys. Chem. C* 116(44), 23653 (2012)
16. Y. Xu, W. Zhao, R. Xu, Y. Shi, and B. Zhang, Synthesis of ultrathin CdS nanosheets as efficient visible-light-driven water splitting photocatalysts for hydrogen evolution, *Chem. Commun.* 49(84), 9803 (2013)
17. Y. Yu, P. Zhang, L. Guo, Z. Chen, Q. Wu, Y. Ding, W. Zheng, and Y. Cao, The design of TiO_2 nanostructures (nanoparticle, nanotube, and nanosheet) and their photocatalytic activity, *J. Phys. Chem. C* 118(24), 12727 (2014)
18. I. Y. Kim, Y. K. Jo, J. M. Lee, L. Wang, and S. J. Hwang, Unique advantages of exfoliated 2D nanosheets for tailoring the functionalities of nanocomposites, *J. Phys. Chem. Lett.* 5(23), 4149 (2014)
19. T. Sagawa, S. Yoshikawa, and H. Imahori, One-dimensional nanostructured semiconducting materials for organic photovoltaics, *J. Phys. Chem. Lett.* 1(7), 1020 (2010)
20. L. Yuan, M. Q. Yang, and Y. J. Xu, Tuning the surface charge of graphene for self-Assembly synthesis of a $SnNb_2O_6$ nanosheet-graphene (2D-2D) nanocomposite with enhanced visible light photoactivity, *Nanoscale* 6(12), 6335 (2014)
21. S. Milner, Polymer brushes, *Science* 251(4996), 905 (1991)
22. A. Halperin, M. Tirrell, and T. P. Lodge, Tethered chains in polymer microstructures, *Adv. Polym. Sci.* 100, 31 (1992)
23. G. S. Grest, Normal and shear forces between polymer brushes, *Adv. Polym. Sci.* 138, 149 (1999)
24. R. C. Advincula, W. J. Brittain, K. C. Caster, and J. Rühe, Polymer Brushes, Weinheim: Wiley VCH, pp 427–440 (2004)
25. G. S. Grest and K. Kremer, Molecular dynamics simulation for polymers in the presence of a heat bath, *Phys. Rev. A* 33(5), 3628 (1986)
26. A. Brasiello, S. Crescitelli, and G. Milano, Development of a coarse-grained model for simulations of tridecanoin liquid-solid phase transitions, *Phys. Chem. Chem. Phys.* 13(37), 16618 (2011)
27. T. Carlsson, N. Kamerlin, G. A. Arteca, and C. Elvingson, Brownian dynamics of a compressed polymer brush model: Off-equilibrium response as a function of surface coverage and compression rate, *Phys. Chem. Chem. Phys.* 13(35), 16084 (2011)
28. I. G. Elliott, T. L. Kuhl, and R. Faller, Molecular simulation study of the structure of high density polymer brushes in good solvent, *Macromolecules* 43(21), 9131 (2010)
29. S. Plimpton, Fast parallel algorithms for short-range molecular dynamics, *J. Comput. Phys.* 117(1), 1 (1995)
30. W. Humphrey, A. Dalke, and K. Schulten, VMD – Visual molecular dynamics, *J. Mol. Graph.* 14(1), 33 (1996)
31. Y. F. Hua, L. X. Zhang, and L. Zhang, Compression-driven migration of nanoparticles in semiflexible polymer brushes, *Polymer* 83(9), 67 (2016)
32. A. Milchev and K. Binder, Unconventional ordering behavior of semi-flexible polymers in dense brushes under compression, *Soft Matter* 10(21), 3783 (2014)
33. G. M. Torrie and J. P. Valleau, Nonphysical sampling distributions in Monte Carlo free-energy estimation: Umbrella sampling, *J. Comput. Phys.* 23(2), 187 (1977)